Collective oscillations and the linear and two-dimensional infrared spectra of inhomogeneous beta-sheets

Dijkstra, AG; Knoester, J

Published in:
Journal of Physical Chemistry B

DOI:
10.1021/jp044141p

Publication date:
2005

Collective Oscillations and the Linear and Two-Dimensional Infrared Spectra of Inhomogeneous β-Sheets

Arend G. Dijkstra and Jasper Knoester*

Institute for Theoretical Physics and Materials Science Centre, University of Groningen, Nijenborgh 4, 9747 AG Groningen, The Netherlands

Received: December 23, 2004; In Final Form: February 28, 2005

We numerically calculate the collective amide I oscillations and the associated linear and two-dimensional infrared (2DIR) spectra for model antiparallel β-sheets and study the effect of inhomogeneity. To visualize the collective vibrational exciton states, a new method is introduced, which proves very useful in classifying the optically dominant states with respect to their symmetry properties and phase relations, even in the absence of exact symmetries. We find that energy (diagonal) and interaction (off-diagonal) disorder may have profoundly different effects on the main peaks in the linear spectrum. We also show that in the 2DIR spectra energy disorder leads to diagonal stretching of the diagonal peaks, while the cross-peaks are typically stretched more horizontally. This offers an explanation for the recently observed overall Z-shape in experimental spectra. Finally, we find that the anharmonic splitting between associated positive and negative features in the 2DIR spectra scales inversely proportionally with the exciton delocalization size imposed by the disorder, thus offering a spectroscopic ruler for this size.

1. Introduction

The study of the structure and dynamics of proteins, in relation to their function, is a problem of central importance for our understanding of elementary processes in living organisms. X-ray crystallography offers a powerful means to study the structure of complex molecules,[1] but is limited to proteins that can be crystallized and, by its very nature, cannot be applied to proteins in their natural environment. Nuclear magnetic resonance (NMR), in particular, its two-dimensional version, does not rely on crystallization and offers an alternative that has been applied with much success.[2] Drawbacks of NMR are its limited time resolution (millisecond) and its reliance on motional narrowing of the NMR lines due to fast reorientational motion.

During the past decade, sparked by the rapidly growing possibilities to control optical and IR pulse sequences at the picosecond and femtosecond time scales, two-dimensional IR (2DIR) and Raman spectroscopies have received increasing attention for the study of molecular structure and dynamics.[3−5] These techniques rely on the structural information contained in (collective) vibrations. In linear (one-dimensional) IR spectra of proteins, this information is often hidden under broad line shapes, resulting from inhomogeneity and the congestion of many vibrational states in a rather narrow spectral region.[6,7] This problem may to some extent be circumvented by performing nonlinear (multipulse) experiments, in which the spectral information is spread along two independent frequency axes, revealing correlations and anharmonic couplings between various vibrational modes. Moreover, these experiments allow for the observation of relatively weak transitions as cross-peaks with strong transitions and for the detection of relative polarization angles between transitions.[5] Also, these multidimensional techniques facilitate the distinction between homogeneous and inhomogeneous relaxation.[8,9]

Over recent years, 2DIR spectroscopy has successfully been applied to a series of small molecules, such as water and small peptides, confirming the potential of the technique to determine structure and dynamics at the molecular level.[10−18] Most recently, several groups have taken up the challenge to study proteins using 2DIR spectroscopy. The most interesting and challenging question is whether this technique may be used to probe the structure of these complex systems and to follow structural changes in real time. To this end, the existence of clear 2DIR markers for structural elements should be investigated. The current focus is on searching for markers of secondary structural elements, especially in the amide I region of the spectrum (around 1650 cm^{-1}). In this context, theoretical and experimental model studies have been performed of α- and 3_{10}-helical structures,[19−22] as well as β-sheets and hairpins.[23,24]

The theoretical study by Cheatum, Tokmakoff, and Knoester,[23] based on an idealized exciton model for the collective amide I oscillations, suggested that the 2DIR spectrum indeed offers markers for β-sheet structure. In particular, it was found that the cross-peaks in this spectrum may be useful to distinguish antiparallel β-sheets from parallel ones as well as β-hairpins. Recent experiments by Demirdöven et al.,[24] in which poly-L-lysine and proteins with different β-sheet content were studied, confirmed the existence of structural markers and the potential of 2DIR spectroscopy to assess the relative β-sheet content. Further experimental studies have even demonstrated the first application of 2DIR spectroscopy to detecting the kinetics of thermal denaturing of a protein.[25]

Of course, the experimentally observed linear and 2DIR spectra of proteins are considerably more complicated and harder to interpret than the ones obtained in idealized model studies. One reason is that in experiment one probes the entire protein, and not an isolated secondary structural element. Moreover, in

* Corresponding author. Fax: 31-50-3634947. E-mail: j.knoester@rug.nl.

10.1021/jp044141p CCC: $30.25
Published on Web 04/23/2005

a real protein, those elements are never ideal. Reproducible as well as random inhomogeneity occurs in the eigenenergies of the individual amide I oscillators (diagonal disorder) and the transfer interactions between them (off-diagonal disorder) as a result of conformational irregularity (for instance, twisting of the sheet) and random solvent shifts. An important source of diagonal disorder (on the order of tens of reciprocal centimeters) is the effect of hydrogen bonding with surrounding protic molecules in the solvent.[10,26−28] The effects of random diagonal disorder on the linear[29] and 2DIR[10] spectra of globular proteins have been considered, while in addition, the effects of conformational disorder on the linear spectra of β-sheets have been modeled.[24]

It is the goal of this paper to perform a systematic study of the effect of random disorder on the linear and 2DIR spectra of model antiparallel β-sheets. Deliberately, we focus on a simple model, in which we still treat the sheet as an idealized plane (finite) lattice and incorporate the disorder in a phenomenological way, instead of taking coordinates for specific proteins from NMR experiments and generating disorder distributions from molecular dynamics simulations. We believe our approach is most useful to investigate the existence of generic spectroscopic markers for β-sheet content, which should not depend too much on the details of the model.

In addition to investigating the one- and two-dimensional spectra, we also pay considerable attention to the nature of the underlying collective vibrational states. In ref 23, it was shown that for homogeneous antiparallel β-hairpins the optically dominant states can be related in a simple way to the (basic) collective oscillations of a single unit cell, consisting of four oscillators. These four basic states are distinguished by the relative phases of the four oscillators. For extended β-sheets, such an identification was argued to be harder, but still was tentatively made for two optically important states (the $|a-\rangle$ and the $|a+\rangle$ states). Hard evidence for this was not given, however. The question concerning the nature of the states gained interest with the clear detection of two dominant spectral peaks in experiment (named the $|\alpha-\rangle$ and $|\alpha+\rangle$ states).[24] In this paper, we introduce a new visualization method of collective states that facilitates and clarifies their proper assignment.

This paper is organized as follows. In section 2, we introduce the model and give the expressions for the spectra in terms of one- and two-quantum eigenstates. Section 3 presents our results and discussion concerning the nature of the one-quantum eigenstates and the linear spectrum. Homogeneous systems are considered in sections 3.1−3.3, while the effects of disorder are the subject of sections 3.4 (diagonal disorder) and 3.5 (off-diagonal disorder). We then switch to a discussion of simulated 2DIR spectra in the presence of disorder (section 4) and demonstrate that this spectrum may be used as an experimental ruler for the exciton delocalization size. Finally, we conclude in section 5.

2. Model and Expressions for the Spectra

Many proteins contain β-sheets as secondary structural elements. They are large, almost two-dimensional structures, consisting of long polymerized polypeptide chains, called strands. The chemical structure of an antiparallel β-sheet is shown in Figure 1. In our convention, the strands run in the horizontal (x) direction. In the vertical (y) direction, strands are held together by hydrogen bonds (dotted lines in Figure 1). The direction perpendicular to the sheet is the z-direction. The

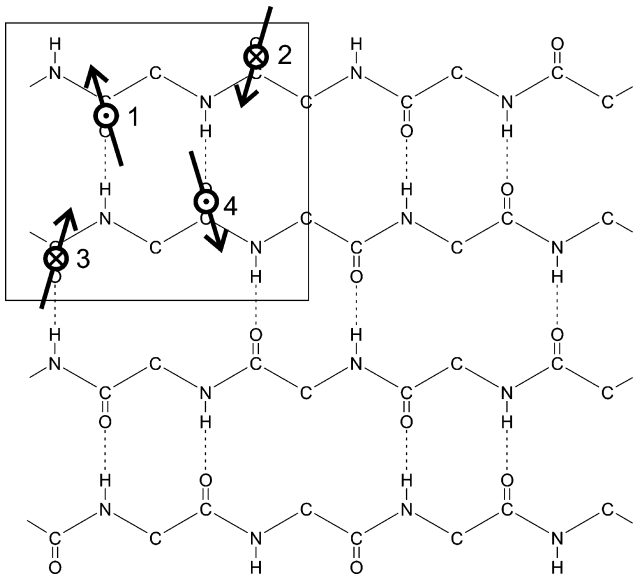

Figure 1. Chemical structure of the antiparallel β-sheet. The sheet is built from strands that run in the horizontal direction. In the vertical direction, the strands are bound together by hydrogen bonds (dashed lines). The structure shown is 2 × 2 unit cells large; a single unit cell is detailed inside the box. The four dipoles in this unit cell are indicated by arrows. The center of the circle on each arrow gives the position of the dipole. The arrow shows its direction in the *xy*-plane. The dipole component in the *z*-direction is indicated by the symbol inside the circle. A dot (cross) means that the normalized dipole has a positive (negative) *z*-component. The components of the dipoles in the plane of the sheet are antisymmetric with respect to inversion of the unit cell; those perpendicular to the sheet are symmetric.

geometry of the sheet is determined by the torsion angles of the strands (ϕ, ψ) and the hydrogen bond length r. Our parameters are (ϕ, ψ) = (−160°, 118°) and r = 0.304 nm. This is the same structural model as was studied by Cheatum, Tokmakoff, and Knoester.[23] As argued in the Introduction, we will focus on idealized planar sheets; we thus neglect strand turns and incomplete unit cells that may occur at the sides of the sheet, as well as twists of the sheet.

The amide I vibration, which is the focus of most current 2DIR studies of small peptides and proteins, is primarily a stretching of the C═O bond in amide groups.[6] At a frequency of 1675 cm^{-1}, it occurs about 100 cm^{-1} away from other vibrational modes, which justifies considering it decoupled from other modes and simplifies its study. The antiparallel β-sheet is seen to contain four amide I oscillators per unit cell, labeled 1 to 4 in Figure 1. For the optical response, each amide group in the sheet is treated as an anharmonic vibrational oscillator. The dipole of the oscillator lies on the C═O bond, 86.8 pm from the carbon atom, and makes an angle of 20° with this bond toward the nitrogen atom. The directions of the dipoles of the four oscillators within the plane of the β-sheet are indicated in Figure 1 by arrows; the very small tilting out of this plane is indicated by a cross (pointing downward) or a dot (pointing upward). Explicit values for the three vector components of the dipoles follow from the geometry of the sheet and are given in Table 1 of ref 23, where also the three-dimensional positions of the oscillators are given.

We will describe the collective amide I vibrations of the sheet by an anharmonic Frenkel exciton Hamiltonian, defined in the site representation.[10] While, in general, this Hamiltonian contains many different terms, we will restrict ourselves to resonant contributions, which conserve the number of vibrational quanta.

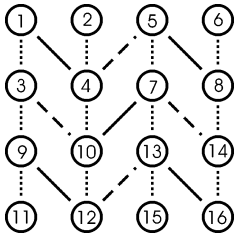

Figure 2. The three strongest interactions obtained in the antiparallel β-sheet within the TDC model. Each circle represents an oscillator. Lines give the interaction strength: $L_{14} = 18.7$ cm^{-1} (solid line), $L_{13} = -7.4$ cm^{-1} (dotted line), and $L_{45} = -4.1$ cm^{-1}. The five next largest interactions that we also accounted for are $L_{23} = 1.5$ cm^{-1}, $L_{15} = L_{26} = L_{37} = L_{48} = 1.3$ cm^{-1}, $L_{49} = L_{27} = 1.1$ cm^{-1}, $L_{25} = L_{47} = 0.8$ cm^{-1}, and $L_{12} = L_{34} = 0.7$ cm^{-1}. Smaller interactions were neglected.

Thus, the coupling between oscillators is given by a bilinear term, describing the transfer of vibrational energy between them. Moreover, for the anharmonic contributions, we restrict ourselves to terms that are diagonal in the site representation, as these are expected to be dominant. Thus, we arrive at the Hamiltonian[10]

$$H = \sum_{n=1}^{N} a_n^\dagger \left(\epsilon_n - \frac{A}{2} a_n^\dagger a_n\right) a_n + \sum_{n,m=1}^{N}{}' J_{nm} a_n^\dagger a_m \qquad (1)$$

where $a_n^\dagger$ and a_n are the Bose creation and annihilation operators, respectively, for an excitation quantum on the nth oscillator and N denotes the total number of oscillators. ϵ_n in the first term of the Hamiltonian represents the transition energy of the nth oscillator. In previous work on β-sheets, all these energies have been taken to be equal, $\epsilon_n = \epsilon_0$. However, this assumption is too restrictive for a sound understanding of experimental data. As was explained in the Introduction, variations in local structure and solvent exposure affect the site energies. We will model such effects by including energetic disorder, taking the site energies randomly and independently from a Gaussian distribution

$$P(\epsilon_n) = \frac{1}{\sigma\sqrt{2\pi}} \exp\left(-\frac{(\epsilon_n - \epsilon_0)^2}{2\sigma^2}\right) \qquad (2)$$

where the standard deviation σ determines the magnitude of the disorder. We will study the effects of this disorder on the collective excited states and the spectra. For the average single-oscillator frequency, we will use $\epsilon_0 = 1675$ cm^{-1}.

Parameter A in the first term of the Hamiltonian is the strength of the anharmonicity; the energy of a doubly excited oscillator is $2\epsilon_n - A$. Throughout this paper, we use $A = 16$ cm^{-1}.[10] Finally, the second term in the Hamiltonian describes interactions between oscillators, where the prime on the summation excludes self-interactions (terms with $n = m$). The interactions are taken from the transition dipole coupling model (TDC).[6,30] Although the validity of this model is disputed and it has been demonstrated that interactions through the peptide backbone may be much stronger than predicted by a TDC calculation,[31,32] no concensus about an alternative parametrization of the interactions in polypeptides exists. We therefore prefer to use one consistent interaction model and include TDC interactions only. The resulting array of oscillators coupled by interactions is shown in Figure 2, where the three strongest interactions have been drawn (solid lines, 18.7 cm^{-1}; dotted lines, -7.4 cm^{-1}, and dashed lines, -4.1 cm^{-1}). Aside from these three interactions, we have also accounted in our calculations for the next five weaker interactions (see caption of Figure 2).

Variations in local structure will obviously also lead to disorder in the interactions. Furthermore, the exact form of the nuclear potential is also not necessarily identical for different oscillators, leading to possible disorder in the anharmonicity parameter A. In the present treatment, we will mostly be concerned with energetic disorder. In section 3.5, we will briefly consider interaction disorder, while variations in the anharmonicity are not included in this paper.

With the knowledge of the sheet geometry and Hamiltonian, we can proceed to calculate the collective energy eigenstates, which may be referred to as (vibrational) excitons. These follow from a simple diagonalization of the Hamiltonian. Because the Hamiltonian (eq 1) does not change the number of excitations in the system, the eigenstates fall apart into different classes, labeled by this number. We expand the eigenstates in the site representation. A one-quantum state $|u\rangle$, from the class of eigenstates with one excitation quantum in the system, can then be written as $|u\rangle = \sum_{n=1}^{N} u_n a_n^\dagger |g\rangle$. A two-quantum state $|w\rangle$ can be decomposed as $|w\rangle = \sum_{n,m\geq n}^{N} (1 + \delta_{nm})^{-1/2} w_{nm} a_n^\dagger a_m^\dagger |g\rangle$. Here, $|g\rangle$ is the ground state, without any excitation quanta, and the coefficients u_n and w_{nm} are the components of the eigenstate in the chosen basis. They follow from an $N \times N$ and an $N(N+1)/2 \times N(N+1)/2$ matrix diagonalization, respectively.

Once the eigenstates and their energies are known, it is straightforward to calculate linear and 2DIR spectra using nonlinear response theory.[33] The linear absorption spectrum as a function of frequency ω is, up to a constant factor, given by

$$A(\omega) = \sum_u \frac{|\boldsymbol{\mu}_{u0}|^2 \gamma}{(\omega - E_u)^2 + \gamma^2} \qquad (3)$$

The summation runs over all one-quantum states $|u\rangle$, which have energies E_u and transition dipole to the ground state $\boldsymbol{\mu}_{u0} = \sum_n u_n \boldsymbol{\mu}_n$, with $\boldsymbol{\mu}_n$ the dipole vector of molecule n. The applied Lorentzian line shape has a homogeneous full width at half-maximum (fwhm) of 2γ.

The 2DIR signal is radiated from a system after interaction with three linearly polarized laser pulses with wave vectors $\mathbf{k}_1$, $\mathbf{k}_2$, and $\mathbf{k}_3$, which arrive at times $t - t_3 - t_2 - t_1$, $t - t_3 - t_2$, and $t - t_3$, respectively. For a fixed time t_2, the signal is measured by scanning t_1 and t_3. The spectrum in the frequency domain is obtained by a double Fourier transform. The variable ω_1 is the Fourier conjugate of t_1, and ω_3 is the conjugate of t_3. The 2DIR spectrum is calculated as the sum of rephasing and non-rephasing contributions. For details concerning the experiment and the calculation of the signal, we refer to refs 5 and 23. Here, we simply state the results. The signal for the rephasing pathways, detected in the $-\mathbf{k}_1 + \mathbf{k}_2 + \mathbf{k}_3$ phase-matched direction, is given by

$$S_1(\omega_1, \omega_3) = \sum_{uv} (o_{uv}^1 + o_{uv}^2) \frac{(\omega_1 - E_u)(\omega_3 - E_v) + \gamma^2}{[(\omega_1 - E_u)^2 + \gamma^2][(\omega_3 - E_v)^2 + \gamma^2]} - \sum_{uvw} o_{uvw}^3 \frac{(\omega_1 - E_u)(\omega_3 - E_{wu}) + \gamma^2}{[(\omega_1 - E_u)^2 + \gamma^2][(\omega_3 - E_{wu})^2 + \gamma^2]} \qquad (4)$$

The non-rephasing diagrams, radiated in the $+\mathbf{k}_1 - \mathbf{k}_2 + \mathbf{k}_3$ direction, yield

$$S_2(\omega_1, \omega_3) = \sum_{uv} o^4_{uv} \frac{-(\omega_1 - E_u)(\omega_3 - E_v) + \gamma^2}{[(\omega_1 - E_u)^2 + \gamma^2][(\omega_3 - E_v)^2 + \gamma^2]} + \sum_{uv} o^5_{uv} \frac{-(\omega_1 - E_u)(\omega_3 - E_u) + \gamma^2}{[(\omega_1 - E_u)^2 + \gamma^2][(\omega_3 - E_u)^2 + \gamma^2]} + \sum_{uvw} o^6_{uvw} \frac{(\omega_1 - E_u)(\omega_3 - E_{wv}) - \gamma^2}{[(\omega_1 - E_u)^2 + \gamma^2][(\omega_3 - E_{wv})^2 + \gamma^2]} \quad (5)$$

In these expressions, the summations over u and v run over all one-quantum states, the summation over w extends over all two-quantum states, and $E_{ab} \equiv E_a - E_b$. The above expressions were derived under the assumption that $t_2 = 0$, which experimentally means that the second and third pulses overlap in time. The signals from rephasing and non-rephasing diagrams are added to obtain the 2DIR correlation spectrum: $S(\omega_1, \omega_3) = S_1(\omega_1, \omega_3) + S_2(\omega_1, \omega_3)$.[5]

The factors o^i in the above expressions for S_1 and S_2 are the orientational parts of the response functions, which account for the specific combination of pulse polarizations, transition dipole orientations, orientational averaging, and orientational relaxation during the experiment. As in ref 23, we will neglect orientational relaxation. As pointed out by Woutersen and Hamm,[11] even for small peptides, molecular rotation is much slower than the time scale of the experiment. Calculating the orientational factors is then a straightforward, albeit tedious, algebraic exercise. The response functions contain four inner products between an electric field vector and a transition dipole. The first three of these derive from the interaction between the polarized input fields and the β-sheet, while the fourth one accounts for the interaction with the polarized heterodyne detection field. We averaged this product of four inner products over an isotropic distribution of orientations of the β-sheet, neglecting, as stated, the possible effects of reorientation during the experiment.

To be specific, we have calculated spectra in the *ZZYY*-polarization for which the third pulse (polarized in the laboratory's *Y*-direction) is perpendicular to the first and second pulses (polarized in the *Z*-direction), while the *Y*-component of the signal is detected. The results for the orientational functions in the *ZZYY*-polarization are

$$o^1_{uv} = o^4_{uv} = \frac{1}{30}[4|\boldsymbol{\mu}_u|^2|\boldsymbol{\mu}_v|^2 - 2(\boldsymbol{\mu}_u \cdot \boldsymbol{\mu}_v)^2] \quad (6)$$

$$o^2_{uv} = o^5_{uv} = \frac{1}{30}[3(\boldsymbol{\mu}_u \cdot \boldsymbol{\mu}_v)^2 - |\boldsymbol{\mu}_u|^2|\boldsymbol{\mu}_v|^2] \quad (7)$$

$$o^3_{uvw} = o^6_{uvw} = \frac{1}{30}[4(\boldsymbol{\mu}_u \cdot \boldsymbol{\mu}_v)(\boldsymbol{\mu}_{wu} \cdot \boldsymbol{\mu}_{wv}) - (\boldsymbol{\mu}_u \cdot \boldsymbol{\mu}_{wu})(\boldsymbol{\mu}_v \cdot \boldsymbol{\mu}_{wv}) - (\boldsymbol{\mu}_u \cdot \boldsymbol{\mu}_{wv})(\boldsymbol{\mu}_v \cdot \boldsymbol{\mu}_{wu})] \quad (8)$$

Here, $\boldsymbol{\mu}_u$ and $\boldsymbol{\mu}_v$ are the transition dipoles between the ground state and the one-quantum states $|u\rangle$ and $|v\rangle$, as introduced below eq 3, while $\boldsymbol{\mu}_{wu}$ is the transition dipole between $|u\rangle$ and the two-quantum state $|w\rangle$ (analogous for $\boldsymbol{\mu}_{wv}$). The latter dipole is easily expressed in terms of the eigenvectors u_n and w_{nm}. In the above expressions, we have normalized the electric field vectors to unity.

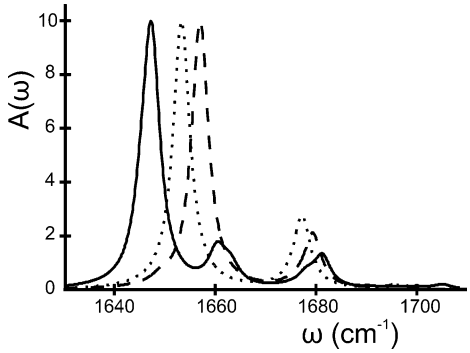

Figure 3. Linear absorption spectra in arbitrary units for a single unit cell of four oscillators (dotted), a 3×1 β-hairpin, existing of a horizontal row of three adjacent unit cells (dashed), and a 3×3 extended β-sheet (solid). In all cases, a value of $\gamma = 2$ cm^{-1} was used for the homogeneous broadening.

3. Results and Discussion: Linear Spectra and One-Quantum Eigenstates

1. Homogeneous Unit Cell. In Figure 3, we present the numerically calculated linear spectra for a single unit cell of four oscillators, the 3×1 β-hairpin (i.e., a system made up of three unit cells in the horizontal direction) and the 3×3 extended β-sheet (having nine unit cells in a square arrangement). In all cases, the system chosen was homogeneous ($\sigma = 0$) and we used a homogeneous line width of $\gamma = 2$ cm^{-1}. These spectra (with somewhat different widths) have been given in ref 23 already. We show them again, because we want to expand on the nature of the states responsible for the various spectral features. In the current subsection, we focus on the unit cell, while the homogeneous hairpin and sheet are discussed in sections 3.2 and 3.3, respectively. The effect of disorder in β-sheets is analyzed in sections 3.4 and 3.5.

The spectrum of the single unit cell (dotted) is dominated by two peaks, occurring at about 1653 and 1677 cm^{-1}. A very faint peak can still be discerned at 1696 cm^{-1}. Considering the inversion symmetry of the unit cell's Hamiltonian with respect to its center (i.e., with respect to interchanging oscillators 1 and 4, and at the same time 2 and 3), the four collective eigenstates underlying these peaks were calculated analytically in ref 23. The two strongest peaks in the spectrum arise from the eigenstates that are antisymmetric with respect to the inversion operation (referred to as *a*-states in ref 23). This is a direct consequence of the fact that the large dipole components are the ones in the plane of the sheet, which are antisymmetric with respect to the inversion operation, as seen in Figure 1. The state underlying the main peak at 1653 cm^{-1} results from the $|a-\rangle$ state, which is the antisymmetric state in which oscillators 1 and 2 have opposite phases. The second peak (at 1677 cm^{-1}) results from the $|a+\rangle$ state, which is antisymmetric with respect to the inversion, and has oscillators 1 and 2 in phase. The *a*-states are polarized in the plane of the sheet.

The other two eigenstates of the unit cell are symmetric with respect to inversion (*s*-states) and have a very small oscillator strength, caused by the small *z*-components of the oscillator dipoles, which are symmetric with respect to the inversion operation. The faint peak at 1696 cm^{-1} results from the $|s-\rangle$ state, which is symmetric, with oscillators 1 and 2 having opposite phases. The $|s+\rangle$ state (at 1674 cm^{-1}) is not visible, because its oscillator strength is too small. Obviously, the *s*-states are polarized perpendicular to the plane of the sheet. We note that the current labeling of the $|s+\rangle$ and $|s-\rangle$ states is interchanged with respect to the one originally given in ref 23, where + and − were used to indicate higher and lower energy,

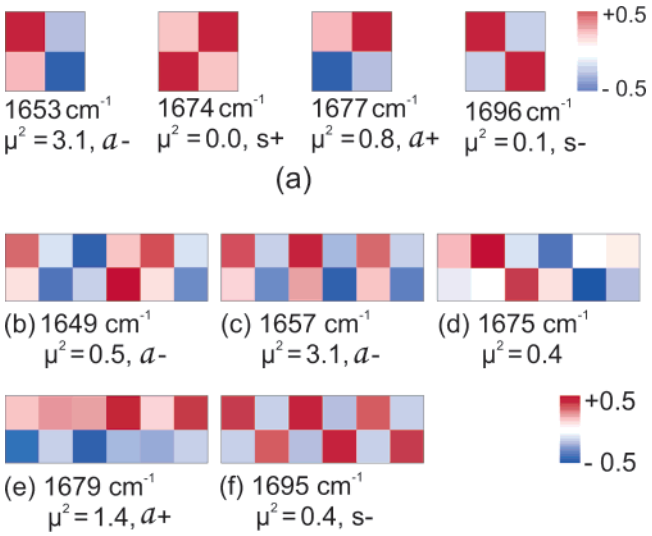

Figure 4. (a) Color maps of the four one-quantum eigenstates ($|a-\rangle$, $|s+\rangle$, $|a+\rangle$, and $|s-\rangle$) of the homogeneous β-sheet unit cell, in order of ascending energy. The colors indicate the value of the wave function on each of the four oscillators of the unit cell, where red stands for positive values and blue for negative components (see legend to the right). Below each state, its energy and the square of its transition dipole to the ground state (in units of the squared dipole of the single oscillator) are given, as well as its symbol. (b)−(f) As in (a), but now for the five states that dominate the dashed spectrum of the homogeneous 3×1 hairpin (twelve oscillators) given in Figure 3.

respectively. For the optically dominant *a*-states, this does not affect the labels.

For future assignment of the eigenstates, it is useful to introduce a visualization of their wave functions that emphasizes the symmetry and phase relations. We do this by making color maps on the plane of the system, as is done in Figure 4a for the four eigenstates of the single unit cell. In this map, each oscillator is represented by a square whose color indicates the eigenstate's component (u_n) on that particular oscillator. Red (blue) stands for a positive (negative) value of u_n, thus distinguishing opposite phases of oscillation on the various oscillators; the intensity of the color indicates the absolute value of u_n. This visualization technique is useful, because it allows us to study the nature of eigenstates by simple inspection and is easily applied to more complicated models of β-sheets. The four color maps given in Figure 4a indeed clearly reflect the symmetry properties and phase relations of the four eigenstates discussed above and will turn out to be useful reference cases for larger color maps to be studied below.

2. Homogeneous Hairpin. In Figure 3, we see that the spectrum of the 3×1 hairpin (dashed) has two dominant peaks, which are slightly blue-shifted relative to the main peaks of the unit cell. A third weak peak around 1695 cm^{-1} is slightly red-shifted relative to the $|s-\rangle$ state of the unit cell. Finally, a fourth feature is seen as a shoulder on the red side of the largest peak. All these peaks were explained analytically, even at a quantitative level, in ref 23 already. It was argued that in hairpins the interactions between adjacent unit cells are so weak that unit cell eigenstates with different symmetry and phase properties are hardly mixed by them. More explicitly, for the $N \times 1$ hairpin, the eigenstates are to a good approximation given by four bands of states, denoted as $|a-\rangle_k$, $|a+\rangle_k$, $|s-\rangle_k$, and $|s+\rangle_k$, with[23]

$$|a-\rangle_k = \sqrt{\frac{2}{N+1}} \sum_{l=1}^{N} \sin\left[\frac{\pi k l}{N+1}\right] |a-\rangle_l \qquad (9)$$

and similar for the other bands. Here, $|a-\rangle_l$ denotes the state in which the lth unit cell is in its basis state $|a-\rangle$, and $k = 1, ..., N$ is the wavenumber of the state. On the basis of estimating interband coupling coefficients, it was argued in ref 23 that the hairpin's eigenstates responsible for the main peaks near 1657, 1679, and 1695 cm^{-1} to a good approximation are given by the $k = 1$ states of the $|a-\rangle$, $|a+\rangle$, and $|s-\rangle$ bands, respectively. The state that contributes the shoulder in the largest peak was associated with the $k = 3$ state of the $|a-\rangle$ band.

The above identification of the eigenstates of hairpins can be made more convincingly by giving their color maps. In order of ascending energy, these maps are given in Figure 4b−f for the four states that are responsible for the spectral features discussed above, as well as for a fifth state that gives a small shoulder in the red wing of the peak near 1679 cm^{-1}. We first note that the five states displayed are either symmetric (b−e) or antisymmetric (f) with respect to inversion relative to the center of the hairpin. The existence of a definite parity with respect to this inversion results from the fact that the Hamiltonian of a homogeneous hairpin (and also a homogeneous extended sheet) has inversion symmetry. The color maps also demonstrate other (approximate) symmetry properties, however. For instance, comparison with Figure 4a clearly shows that the state displayed in Figure 4c, mainly responsible for the spectral peak at 1657 cm^{-1}, repeats the color pattern of the $|a-\rangle$ basis state in each of its three unit cells. Thus, inside each unit cell, the cell symmetry and phase relations follow those of the $|a-\rangle$ state, with the same overall sign of the phase for all three unit cells. This confirms that indeed this state to a good approximation is the $|a-\rangle_{k=1}$ state. Similarly, Figure 4e,f clearly exhibits the symmetries and phase relations appropriate for the $|a+\rangle_{k=1}$ and $|s-\rangle_{k=1}$ states, respectively. The other two states at first sight have less regular color maps. Upon closer inspection, however, Figure 4b in each of its unit cells has the (approximate) symmetry and phase relations belonging to the $|a-\rangle$ basis state, with the middle cell having an opposite overall phase relative to the outer two. Thus, this state has the symmetries and phase relations appropriate for $|a-\rangle_{k=3}$, confirming its assignment made in ref 23. Likewise, the remaining state in Figure 4d has the phase relations that belong to $|a+\rangle_{k=3}$, although in this case the exact amplitudes on each of the oscillators, while having the correct signs, considerably deviate from the ideal $|a+\rangle_{k=3}$ state, probably due to mixing with the close-lying $|s+\rangle$-type basis states of the three unit cells.

We have studied the color maps for the four optically dominant eigenstates of hairpins of up to six unit cells long and found that they always have the phase symmetries and phase relations appropriate to the states $|a-\rangle_{k=1}$, $|a+\rangle_{k=1}$, $|a-\rangle_{k=3}$, and $|s-\rangle_{k=1}$ (in order of descending oscillator strength). The $|a-\rangle_{k=3}$-type state was found to shift from 1649 to 1654 cm^{-1} with increasing hairpin length, consistent with the dispersion of the $|a-\rangle$ band found in ref 23. The three other states vary very little in energy, reflecting the weak intercell interactions.

Owing to the symmetry of the various dipole components on the oscillators, only states that are (anti)symmetric with respect to both the global symmetry and the cell symmetry will have a large oscillator strength. A state that is perfectly symmetric (antisymmetric) with respect to the global symmetry and perfectly antisymmetric (symmetric) with respect to the unit cell symmetry has no oscillator strength at all. Quite generally, the low-wavenumber states, in which no overall phase differences exist between different unit cells, dominate the spectrum. These statements also hold for extended β-sheets (see below). In practice, cell symmetries are not exact, although, as we have

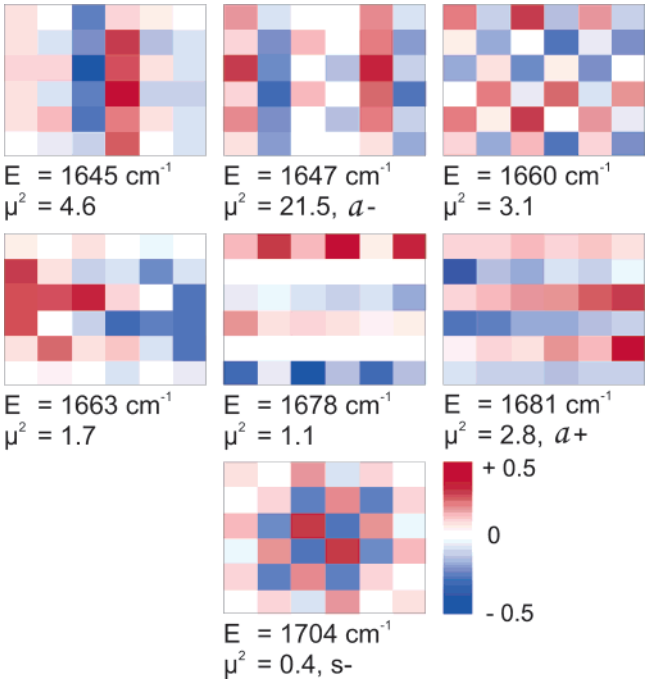

Figure 5. Color maps of the 7 one-quantum eigenstates in a homogeneous 3 × 3 unit cell β-sheet (36 oscillators) that have a significant dipole to the ground state.

seen above, for hairpins they survive the intercell interactions to a very good approximation. Finally, the polarization of the states is governed entirely by the global symmetry. States that are antisymmetric (symmetric) with respect to global inversion have a transition dipole to the ground state that is oriented parallel to (perpendicular to) the plane of the hairpin. In practice, this means that, as for the isolated unit cell, all *a*-type (*s*-type) states are polarized parallel (perpendicular) to the plane of the system.

3. Homogeneous Sheet. The spectrum of the 3 × 3 sheet (solid line in Figure 3) shows more structure than the one for hairpins. The main peak is now red-shifted relative to the $|a-\rangle$ state of the unit cell and the feature around 1680 cm^{-1} appears to consist of two closely spaced peaks, while a new feature (with substructure) has emerged just above 1660 cm^{-1}. The weak peak near 1700 cm^{-1} is shifted to the blue relative to the unit cell and the hairpin spectrum. As was noted in ref 23, assigning the spectral peaks for extended sheets is more complicated than for hairpins. The reason is that in extended sheets strong interactions exist between unit cells (for instance, the interaction between oscillators 7 and 10 in Figure 2 and the interactions between 3 and 9 and between 4 and 10).

First, these stronger interactions lead to wider exciton bands than in the case of hairpins, as is clear from the separation between highest and lowest peaks in Figure 3. Second, and more importantly, as these interactions are not weak relative to the energy differences between the four eigenstates of the isolated unit cell, these states will be mixed in extended sheets. Thus, one expects that in extended sheets the intracell parity and phase properties are mixed, making it more difficult to associate the spectral peaks with unit cell eigenstates, such as $|a\pm\rangle$. Despite this, in ref 23, the dominant state at about 1645 cm^{-1} was tentatively labeled as an $|a-\rangle$-type state,[34] while the one near 1680 cm^{-1} was associated with $|a+\rangle$.

The color maps introduced above allow us to asses in more detail to what extent the unit cell symmetries persist for extended sheets. The seven eigenstates of the 3 × 3 sheet with the largest oscillator strengths are depicted in Figure 5 in order of ascending energy. Because the global inversion symmetry is exact for this system, all eigenstates are either antisymmetric (the first six) or symmetric (the last one) with respect to inversion in the sheet's center. As noted above, this means that the first six states are polarized in the plane of the sheet, while the seventh is polarized perpendicular to it. In addition to the global symmetry, several states in Figure 5 show rather consistent intracell parity and phase relations. In particular, the second state (energy 1647.2 cm^{-1}) to a good approximation has $|a-\rangle$ character: seven unit cells out of nine have $a-$ symmetry. This justifies its identification as an $|a-\rangle$-type state. The strong $a-$ character is immediately recognized from the fact that the color map resembles an array of six columns that alternate in color when going from left to right. The fact that no overall phase changes occur between unit cells (i.e., the same cell pattern is repeated) indicates that this resembles the smallest-wavevector state with $a-$ character, with the strongest transition dipole.

Studying more general $N \times N$ sheets, we have found that always by far the strongest state in the spectrum occurs near 1645 cm^{-1}. It always is antisymmetric with respect to global inversion. Moreover, for N even, this state to an excellent approximation has $a-$ symmetry (with regard to the phases of the oscillators): all unit cells have the required $a-$ symmetry for N up to 14, while for $N = 16$, only 4 (out of 256) cells have symmetry that is not $a-$. For N odd, the cell symmetry is not present in all unit cells, as we already found above for $N = 3$.

A second strong peak in the sheet spectra is found near 1680 cm^{-1}. As is illustrated in Figure 5, it is mainly caused by the transition at 1680.7 cm^{-1}, which to a very good approximation has $a+$ symmetry. Note the clear difference between the color map of this state (a stack of rows that alternate in color from top to bottom) and the one at 1647 cm^{-1} (alternating columns), illustrating the usefulness of these maps. Centered around 1660 cm^{-1} are several states with considerable oscillator strengths. The one at 1660.1 cm^{-1} still has a large $a-$ character and can be interpreted as a higher-wavevector state in the $|a-\rangle$ band; this identification is confirmed by the fact that relative phase changes occur between unit cells in the vertical (y) direction. By contrast, the state at 1662.7 cm^{-1} has no consistent intracell parity and phase relation, implying that it arises from strong mixing of unit cell eigenstates. All states dealt with so far have negative parity with respect to the global inversion symmetry and therefore are polarized within the xy-plane. Only the very faint state near 1705 cm^{-1} has positive global parity and is polarized in the z-direction. Notice that the color map of this state clearly has a checkerboard pattern, indicative of the lowest-wave-vector state with a strong $s-$ character.

We finally notice that, if we would have imposed periodic boundary conditions, the eigenstates would always preserve clear parity labels, both with respect to the global symmetry and with respect to phase relations within cells.[35−37] The reason is that all unit cells would be equivalent then, and for the optically allowed states, no phase differences would occur between unit cells, because of the $\mathbf{q} = 0$ selection rule imposed by the translational symmetry. As was noted in ref 23, however, the use of periodic boundary conditions on extended sheets leads to significant qualitative errors, especially in the polarization properties of the dominant ($a+$ and $a-$ type) states.

4. Sheet with Diagonal Disorder. As mentioned in the Introduction, disorder plays an important role in understanding experimental spectra. In this subsection, we will discuss the effect of diagonal disorder on the linear spectrum of extended β-sheets. Figure 6 shows the linear spectrum for a 3 × 3 sheet in the absence of disorder (solid line) and for two values of the

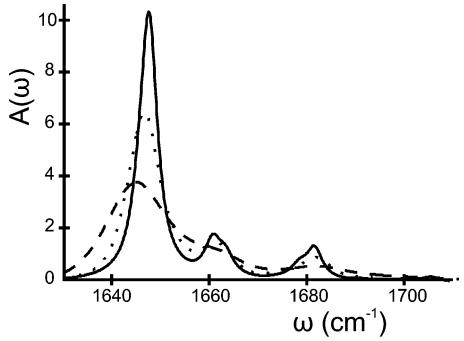

Figure 6. Linear absorption spectrum, in arbitrary units, of a 3 × 3 β-sheet in the absence of disorder (solid) and with diagonal disorder of strength $\sigma = 5$ cm^{-1} (dotted) and $\sigma = 10$ cm^{-1} (dashed). Spectra with disorder were obtained through Monte Carlo simulations, averaging over 10 000 disorder realizations. In all spectra, a value of $\gamma = 2$ cm^{-1} was used for the homogeneous broadening of individual exciton transitions. The three spectra have equal area, reflecting the conservation of the total oscillator strength. The disorder-induced broadening of spectral lines and the red-shift of the dominant $|a-\rangle$ peak are clearly visible.

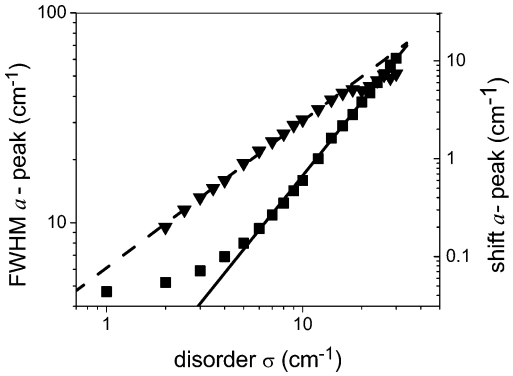

Figure 7. Dependence of the width (squares) and shift (triangles) of the $|a-\rangle$ peak in the linear absorption spectrum of the 3 × 3 unit cell β-sheet on the strength σ of the diagonal disorder. The lines indicate power-law fits, for which the parameters are given in the text.

disorder strength: $\sigma = 5$ cm^{-1} (dotted) and $\sigma = 10$ cm^{-1} (dashed). In all cases, the homogeneous width was set to $\gamma = 2$ cm^{-1}.

The observed changes due to disorder are quite typical. The first obvious effect is a broadening of the spectral lines. This results from the fact that disorder breaks the inversion and approximate translational symmetry in the system; it thus mixes the unperturbed eigenstates and breaks the optical selection rules for the excitons: more collective states become strongly dipole-allowed. We calculated the fwhm W of the strongest peak (the $|a-\rangle$ peak) as a function of the disorder strength σ (keeping the system size constant at 3 × 3 unit cells). For 5 cm^{-1} $\leq \sigma \leq$ 30 cm^{-1}, which is significantly larger than the homogeneous half-width of 2 cm^{-1}, we observe power-law behavior: $W \approx a\sigma^b$ (squares in Figure 7). When both W and σ are expressed in wavenumbers, a least-squares fit yields $a = 1.1$ and $b = 1.2$. Power-law scaling of the optical line width of energetically disordered exciton systems has been found previously by Schreiber and Toyozawa[38] and Fidder, Knoester, and Wiersma.[39] These authors reported $b = {}^4/_3$ for one-dimensional systems and $b = 2$ for two-dimensional systems, in both cases with equal orientation of all oscillator dipoles. Comparing our result for b with the cited values, we observe that line broadening in β-sheets does not scale as in a two-dimensional system. This is not surprising, because the interactions in the sheet render the system non-isotropic. In addition, the occurrence of four different dipole orientations leads to four interwoven exciton bands, which also leads to a different line broadening.

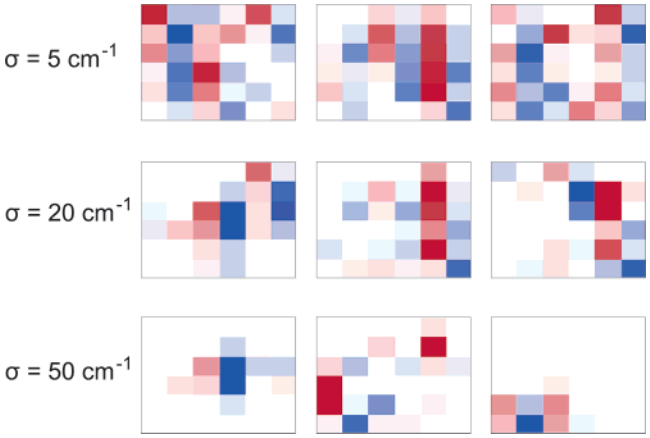

Figure 8. Color maps of the one-quantum eigenstate with the largest dipole to the ground state for a disordered 3 × 3 unit cell β-sheet. Three values of the disorder were considered ($\sigma = 5$, 20, and 50 cm^{-1} from top to bottom), and for each σ value, three disorder configurations were generated randomly (left to right). For each of these realizations, the optically strongest state is shown. Color coding is as in Figure 5.

Apart from line broadening, disorder also causes the energy separation between the two main spectral peaks (the $|a-\rangle$ and $|a+\rangle$ peaks) to increase. This is visible in Figure 6 mainly as a red-shift of the $|a-\rangle$ peak. The peak shift, caused by disorder-induced coupling between the homogeneous eigenstates, is well-known for J aggregates.[38,39] The red-shift S of the $|a-\rangle$ state in our β-sheet model (triangles in Figure 7) is observed to follow power-law scaling for $\sigma \leq 17$ cm^{-1}: $S \propto \sigma^b$, with $b = 1.5$ from a least-squares fit. Again, the result can be compared with linear aggregates, where the exponent is found to be slightly smaller, $b = 1.35$.[39] For larger values of the disorder, the peak shift does not increase anymore, but even decreases somewhat. This effect can be understood by realizing that, for these large values of σ, the peaks broaden so much that they start to overlap. In particular, the $|a-\rangle$ peak starts to merge with the higher-energy peaks. The growing overlap displaces the weight of the total peak to the high-energy side, causing a blue-shift that compensates for the disorder-induced red-shift. The net effect is a deviation from the power-law behavior which we observed for smaller disorder values.

Finally, we analyze the nature of the eigenstates in the presence of disorder. To this end, we plot in Figure 8 the color maps of the state with the largest transition dipole to the ground state that occurs within three randomly chosen disorder realizations for $\sigma = 5$, 20, and 50 cm^{-1}. For small disorder, we expect these dominant states to be of the $|a-\rangle$ type. Indeed, for the three states found for $\sigma = 5$ cm^{-1}, we still see an overall color pattern that resembles the alternating red and blue columns of the state at 1647.2 cm^{-1} in Figure 5. The fact that we are still dealing with weak disorder is clear from the fact that all three states considered are still strongly delocalized over the entire sheet. Even the global inversion symmetry seems not to be broken very strongly, implying that these states are mostly polarized within the plane of the sheet. The disorder of 5 cm^{-1} is too small to cause strong mixing between the lowest-lying $|a-\rangle$-type state and states of different symmetries, and the broadened low-energy absorption peak may still be referred to as an $|a-\rangle$ peak.

At $\sigma = 20$ cm^{-1}, we see from the many white or very light sites in the color maps that the states tend to get more localized

on a part of the sheet. Anderson localization of exciton states is well-known in the field of electronic excitons in *J* aggregates and semiconductors, and in many such systems, the exciton localization size is considered an important microscopic quantity whose measurement has attracted much attention.[40−42] Also, for exciton models of globular proteins, localization has been studied.[10,29] Even though at $\sigma = 20$ cm^{-1} the exciton states are localized in our model β-sheets and their global symmetry is lost, we see that within their localization area their color maps still bear a marked (though not perfect) resemblance to the alternating red and blue column pattern. This justifies us to still refer to these states as $|a-\rangle$-type states and also, in hindsight, justifies us to identify the strong $|\alpha-\rangle$ absorption peak defined in ref 24 as an $|a-\rangle$-type peak.

For $\sigma = 50$ cm^{-1}, the states are strongly localized. Even in this case, however, we recognize that locally the strongly dipole-allowed states seem to carry a fair $|a-\rangle$-type character. It should be noted, however, that for this large value of σ no distinction can be made between different absorption bands anymore, so that we cannot speak of an $|a-\rangle$ peak in the spectrum. The fact that we still only found states that locally look like the $|a-\rangle$ states, directly results from the fact that selecting the largest dipole automatically selects phases between neighboring oscillators that also apply to the $|a-\rangle$-type states.

We notice that a more complete study of the nature of the eigenstates in the presence of disorder requires a more systematic investigation of the energy dependence of certain moments of the wave functions. A good choice would be to consider the autocorrelation function of the wave function as a function of energy.[43] This would allow one to distinguish whether states underlying the strongest absorption bands indeed may be referred to in a statistically meaningful way as $|a-\rangle$ or $|a+\rangle$ states. Recently, a similar study was performed to investigate the chiral behavior of exciton states in helical cylinders.[44]

5. Off-Diagonal Disorder. We have seen that, for $\sigma \leq 17$ cm^{-1}, the $|a-\rangle$ peak shifts to lower energy with increasing disorder strength. While for energetic disorder this is the normal behavior for the lower band edge states, for disorder in the interactions J_{nm}, this need not be the case. Such disorder naturally arises from conformational disorder: small random deviations of oscillator positions and dipoles from their regular values lead to random changes in the TDC interactions. This type of disorder was simulated by Demirdöven et al.,[24] who applied random Gaussian shifts of the oscillator positions. They found that the $|a-\rangle$ peak was broadened and shifted to the blue as a result of disorder, while the $|a+\rangle$ peak hardly changed in position and width. No explanation was offered, except that the change in position of the $|a-\rangle$ peak was ascribed mainly to fluctuations in the interstrand distances. Our study shows that this is not correct.

As a simple example, we have considered interaction disorder in a single unit cell by varying the positions of the four oscillators. The displacements are random and uncorrelated. We first look at variations in the *xy*-plane, by taking the absolute value of the displacement from a Gaussian distribution and its direction from a uniform distribution. Figure 9 shows the resulting linear spectra for different disorder strengths, where for clarity the spectra have been scaled to equal amplitude of the $|a-\rangle$ peak. From the figure, we observe that the $|a-\rangle$ peak shifts to the blue and strongly broadens, while the $|a+\rangle$ peak shifts slightly to the red and hardly broadens. The explanation for the shifts is that the conformational disorder decreases the average TDC strength, thus giving smaller exciton dispersions and keeping the average exciton transitions closer to the single-oscillator frequency. Because for the $|a+\rangle$-type states, the various interactions largely cancel each other (which is why this state occurs so close to the single-oscillator energy), the net effect of disorder in these interactions on the line shift is also smaller. For the same reason, the fluctuations in the strengths of the interactions have a much smaller effect on fluctuations in the position of the $|a+\rangle$ state than the $|a-\rangle$ state, leading to the considerably smaller line broadening of the $|a+\rangle$ peak.

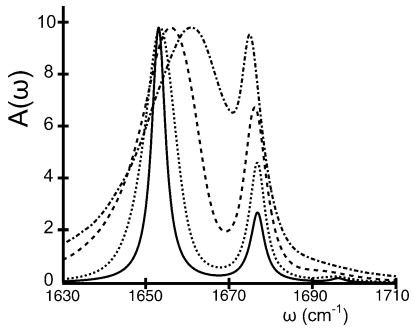

Figure 9. Spectra of a single unit cell with disorder in the oscillator positions. Oscillators have been randomly displaced in the *xy*-plane with a uniform distribution of the angle of displacement and a Gaussian distribution of the standard deviation *s* in the distance. The four spectra correspond to $s = 0$ (solid), $s = 17.3$ pm (dotted), $s = 50$ pm (dashed), and $s = 100$ pm (dash−dotted). Spectra have been averaged over 50 000 disorder realizations. In all cases, a value of $\gamma = 2$ cm^{-1} was used for the homogeneous broadening of individual exciton transitions. We observe that the excitonic band narrows with increasing disorder, resulting from a blue-shift of the $|a-\rangle$ peak.

To get a better understanding of the origin of the strong blue-shift of the $|a-\rangle$ peak, we also randomly varied the oscillator positions in only one of the spatial directions. In the resulting spectra (not shown), we observe that fluctuations in the *x*-direction almost entirely explain the blue-shift of this peak, while variations in the interstrand spacing (i.e., Gaussian disorder in the *y*-direction) have almost no effect on the position of this peak. This conclusion is in marked contrast to the suggestion made in ref 24 that the interstrand distances are the crucial quantities. We also found that disorder in the *z*-component of the oscillator positions leads to a small blue-shift of the $|a-\rangle$ peak.

4. Results and Discussion: 2DIR Spectra of Extended Sheets

Figure 10 shows the calculated 2DIR correlation spectrum in the *ZZYY*-polarization without disorder (panel (a)) and with Gaussian diagonal disorder of strength $\sigma = 10$ cm^{-1} (panel (b)). In both plots, a homogeneous half-width at half-maximum (hwhm) of $\gamma = 2$ cm^{-1} has been used. Panel (b) was generated by averaging over 500 disorder realizations. The spectrum for the homogeneous system was discussed at considerable length in ref 23. It contains positive peaks (red and yellow), resulting from bleaching and stimulated emission contributions, and associated negative peaks (blue), resulting from induced-absorption processes to two-quantum eigenstates. As a result of the anharmonicity of the oscillators, the induced-absorption peaks are red-shifted along the ω_3 direction relative to the associated positive features. The spectrum shows such pairs of positive and negative features both at the diagonal of the (ω_1, ω_3) plane, where ω_1 and ω_3 basically probe the same exciton, as well as outside the diagonal, where the correlation between two different exciton states is seen as cross-peak. As was argued

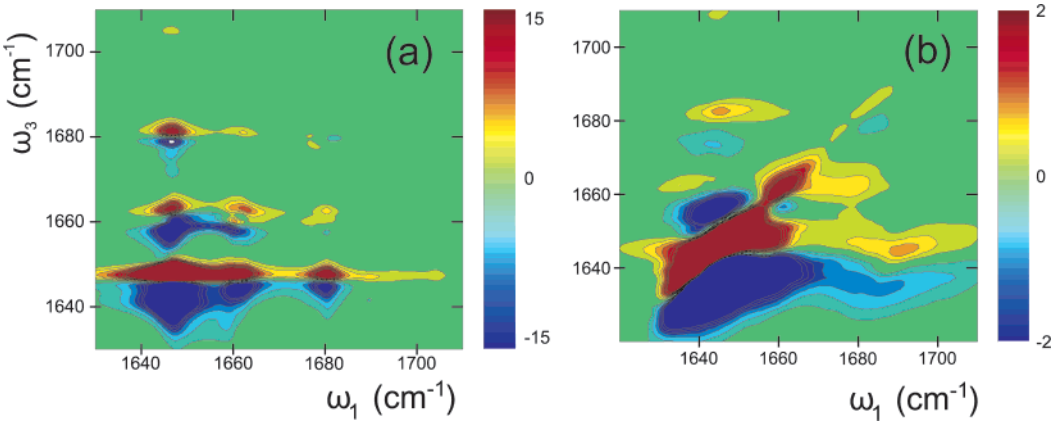

Figure 10. 2DIR spectra in the *ZZYY* polarization for a homogeneous 3 × 3 unit cell β sheet (a) and the same sheet with Gaussian diagonal disorder of standard deviation $\sigma = 10$ cm^{-1} (b). In both spectra, we used $\gamma = 2$ cm^{-1} for the homogeneous broadening of the exciton transitions. To generate the spectrum in (b), we averaged over 500 disorder realizations.

in ref 23, especially, the cross-peaks seem to be sensitive probes for secondary structure in proteins. In the calculated spectra for the homogeneous sheet, we clearly see the cross-peaks between $|a-\rangle$ and $|a+\rangle$, between $|a-\rangle$ and $|s-\rangle$, and between $|a-\rangle$ and the states around 1660 cm^{-1}. The fact that all features in the 2DIR spectra are extended in the ω_1 direction, and not in the ω_3 direction, results from the homogeneous broadening, which merges close-lying peaks of the same sign in the spectrum. In the ω_3 direction, the close-lying pairs of positive and associated negative contributions, even after homogeneous broadening, still stay visible as separate peaks of opposite sign (albeit with less amplitude with increasing value of γ).

As expected from the linear absorption spectrum, we observe that the features in the 2DIR spectrum broaden when disorder is present. The diagonal peaks strongly stretch along the diagonal, leading to a rather featureless diagonal ridge. As in the case of the linear spectrum, the broadening results from many exciton transitions obtaining a large transition dipole as a consequence of the symmetry breaking by the random disorder. The fact that diagonal peaks are slanted along the diagonal direction results from the fact that our model treats the disorder as purely static. Thus, the energy of a particular exciton state $|u\rangle$ stays constant throughout the experiment, giving rise to a bleaching resonance at $(\omega_1, \omega_3) = (E_u, E_u)$.

Disorder also has a clear influence on the cross-peaks, which are seen to further extend along the ω_1 direction than in the homogeneous case. This results from the extra broadening, which, like the homogeneous broadening, leads to merging peaks of the same sign in the two-dimensional spectrum, while preserving the separate positive and negative peaks along the ω_3 direction. We observe that the strong cross-peak positioned around $(\omega_1, \omega_3) \approx (1685$ cm^{-1}, 1640 cm$^{-1})$ is slanted out of the horizontal direction toward the diagonal direction. This results from the fact that, within a certain realization of the disorder configuration, a positive correlation exists between the energies of different exciton transitions, for instance, of the $|a-\rangle$- and $|a+\rangle$-type transitions. This correlation derives from the fact that, in a finite system, the average of the N randomly chosen ϵ_n values is not exactly ϵ_0, but deviates from this mean by an amount that is different for each disorder realization. This deviation in the average transition energy shifts all exciton transitions within a certain disorder realization by the same amount (i.e., creates a positive correlation between the exciton energies within a given disorder realization). We note that this correlation is not perfect, as has been shown explicitly for the case of excitons in linear molecular aggregates in ref 45, which explains why, as opposed to the diagonal peaks, the cross-peak is not oriented exactly along the diagonal direction of the spectrum. Also for the other cross-peaks observed in Figure 10b, this correlation effect is visible, albeit only weakly for the peak around $(\omega_1, \omega_3) = (1640$ cm^{-1}, 1680 cm$^{-1})$.

Generally speaking, the slanting of (cross-)peaks in 2DIR spectra away from the ω_1 axis is indicative of the presence of static disorder;[46] dynamic fluctuations on time scales short compared to the pulses or t_2 tend to wash out the correlations necessary for this slanting, as we have also seen in the homogeneous limit, Figure 10a. As we observe from our simulations (and explained above), even for purely static disorder, the excitonic cross-peaks tend to lie closer along the ω_1 direction (less diagonal slanting) than the diagonal peaks. The combined effect of diagonal peaks being strongly stretched along the diagonal of the 2D spectrum and cross-peaks being more elongated along the ω_1 direction leads to an overall spectrum that resembles a Z. This Z-shape may be taken as the spectral signature for the presence of β-sheets in a protein.

Recently, Z-shaped 2DIR spectra have indeed been observed experimentally for poly-L-lysine, as well as for β-sheet containing proteins, such as concanavalin A and ribonuclease A.[24] Our simulations show that the presence of disorder offers a natural explanation for the observed Z-shape. In contrast to our results, however, the experimental spectra seem to exhibit no slanting of the cross-peaks at all, while the main diagonal peak is clearly directed along the diagonal. The explanation may well be that in the experiment the main diagonal peak, associated with $|a-\rangle$-type transitions, is mainly inhomogeneously broadened, while the cross-peaks, also involving $|a+\rangle$-type states, mainly undergo homogeneous (dynamic) broadening. As we have observed in Figure 9, in particular, the presence of conformational disorder may lead to a strong reduction of the inhomogeneous broadening of the $|a+\rangle$ transitions as compared to the $|a-\rangle$ transitions. This fact and the already noted absence of perfect correlation in the inhomogeneous shifts of the energies of different exciton states may easily explain that the cross-peaks are stretched along the ω_1 direction, while the main diagonal peak is slanted along the diagonal.

As was suggested in earlier work,[23] the splitting between positive and associated negative peaks in the 2DIR spectrum is expected to contain information about the number of oscillators that share an excitation (i.e., about the exciton delocalization size L). The reason is that this splitting finds its origin in the

anharmonic term of the Hamiltonian, $H_{\mathrm{anh}} = -(A/2)\sum_{n=1}^{N} a_n^\dagger a_n^\dagger a_n a_n$, which roughly stated adds the fourth powers of the amplitudes of the exciton states on all oscillators. For a state shared by L oscillators, this amplitude scales as $1/\sqrt{L}$, leading to an expected anharmonic splitting $\Delta \approx A/L$ between the negative induced-absorption peak and the associated positive bleaching peak (the latter one being higher in energy). Similarly, using simple statistical arguments, Hochstrasser and co-workers arrived at $\Delta = 2A/(L+1)$ for L-coupled oscillators.[10]

It is useful to derive the expected scaling from perturbative arguments, instead of the above heuristic ones. In the absence of H_{anh}, there is no anharmonic shift and the two-quantum eigenstates are just the two-boson states $|u, v\rangle = \sum_{n,m} u_n v_m a_n^\dagger a_m^\dagger |g\rangle$. Let us consider the effect of H_{anh} on the excitonic overtone $|2u\rangle = (1/\sqrt{2})\sum_{n,m} u_n u_m a_n^\dagger a_m^\dagger |g\rangle$, where the prefactor $1/\sqrt{2}$ ensures proper normalization (the one-quantum eigenvector u_n is assumed to be normalized to unity). To first order in H_{anh}, the anharmonic shift is then given by

$$\Delta_1 = -\langle 2u|H_{\mathrm{anh}}|2u\rangle = A\sum_n |u_n|^4 = \frac{A}{L} \qquad (10)$$

where $L \equiv (\sum_n |u_n|^4)^{-1}$ is now the participation ratio, a well-known measure of the one-particle delocalization size in disordered systems.[47] This confirms the scaling postulated in ref 23. One may argue, however, that for our system the value of A does not justify a first-order treatment. To estimate higher-order effects, we also consider the second-order shift of the energy of the state $|2u\rangle$, which reads

$$\Delta_2 = -2A^2\sum_{u',u''} \frac{|\sum_n u_n^{*2} u'_n u''_n|^2}{2E_u - E_{u'} - E_{u''}} \qquad (11)$$

If we consider this shift, in particular, for states $|u\rangle$ that occur at the bottom of the exciton band, such as the spectrally dominant $|a-\rangle$-type states, we see that Δ_2 is positive (i.e., it increases the energy spacing between the bleaching and induced-absorption peaks). We can further estimate Δ_2 by approximating the energy denominator in eq 11 by B, where B is on the order of the total exciton bandwidth. The summations over u' and u'' can then be performed using the closure relation on these wave functions, leading to $\Delta_2 = 2A^2/(BL)$, where again L is defined as the participation ratio. Because, for the system under consideration, $2A = 32$ cm^{-1}, while B is on the order of 60 cm^{-1}, we see that $\Delta_2 \approx \Delta_1/2$. It is likely that yet higher-order terms add similar contributions, leaving us with an expected scaling of $\Delta = cA/L$ with c on the order of unity.

Using our numerical simulations of the 2D spectrum, we have investigated whether indeed such simple scaling relations exist between the peak splitting Δ and the delocalization size of the one-quantum states. Because the spectrum is two-dimensional, one may define the splitting between the positive and negative peaks in various ways. We have defined the splitting Δ_{a-} as the frequency separation between the negative minimum and the positive maximum in a slice through the 2D spectrum at $\omega_1 = \Omega$. Here, Ω is the position of the maximum of the main $(a-)$ peak in the linear absorption spectrum. Note that, because of the broadening of the exciton band with increasing disorder strength, Ω is different for each value of the disorder strength σ. In Figure 11, the splitting obtained from this procedure over a range of values of the disorder strength (1 cm^{-1} $\leq \sigma \leq$ 30 cm^{-1}) is plotted against the delocalization size L. The latter was

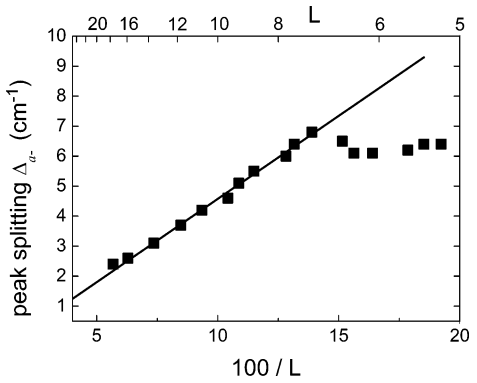

Figure 11. Splitting between the positive and negative parts of the diagonal $|a-\rangle$ peak in the 2DIR spectrum vs the inverse localization size $1/L$, with L obtained from the average participation ratio. The data (squares) have been obtained for a 3×3 sheet, using the *ZZYY* polarization and taking $\gamma = 2$ cm^{-1}. For each σ value, the spectrum was obtained by averaging over 500 disorder realizations. The solid line is the best linear fit for $L \geq 8$ (see text for slope).

calculated as the average participation ratio of the exciton states at energy Ω[47]

$$L = \langle \sum_u (\sum_{n=1}^{N} u_n^4)^{-1} \delta(\Omega - E_u)\rangle / \langle \sum_u \delta(\Omega - E_u)\rangle \qquad (12)$$

where $\langle ... \rangle$ indicates the disorder average.

From Figure 11, it is clear that, as long as the disorder strength is not too large (i.e., the localization size is not too small), the expected relationship

$$\Delta_{a-} = cA/L \qquad (13)$$

holds. For $L \geq 8$, corresponding to $\sigma \leq 10$ cm^{-1}, we find $c = 3.4$. For larger values of the disorder strength, the peak splitting shows a sharp decrease. This unexpected decrease is entirely due to the behavior of the negative peak and is probably caused by interference effects with other spectral features, similar to the non-monotonic behavior of the peak shift S as a function of disorder strength observed in section 3.4.

The scaling relation eq 13 provides a tool to estimate the exciton delocalization size in β-sheets from the experimentally observed peak splitting, provided that static disorder dominates the spectral broadening. For electronic excitations in linear molecular aggregates, it has been demonstrated that the two-color pump−probe spectrum provides a similar spectroscopic ruler for the exciton delocalization size.[40,48]

To close this section, we note that in various publications the participation ratio has been used in a slightly different way, defining L as the inverse of the average of $\sum_{n=1}^{N} u_n^4$.[38,39] Both definitions correctly monitor the localization behavior, though their numerical values differ, in particular, for larger disorder strengths, where distribution functions get broader. We have checked that the alternative definition for L still gives the linear scaling of eq 13, with $c = 3.1$.

5. Conclusions

In this paper, we numerically studied the effects of static disorder on the collective vibrational exciton states of the amide I type in antiparallel β-sheets and the corresponding linear and two-dimensional IR spectra. We mostly focused on energetic (diagonal) disorder. To analyze the nature of the exciton states, we introduced a new visualization technique in which the exciton wave function is represented as a two-dimensional color

map. This color map facilitates recognizing symmetries of the wave function and phase relations between various oscillators in the sheet. Using these maps, we confirmed that for homogeneous β-hairpins the collective states to a very good approximation separate into four different bands that have a one-to-one correspondence to the four eigenstates ($|a-\rangle$, $|a+\rangle$, $|s-\rangle$, $|s+\rangle$) of a single unit cell in the sheet.

For β-sheets that are extended in both directions, this identification is less ideal, as strong interactions between different unit cells mix the various types of cell eigenstates. Still, using the color maps, we have been able to demonstrate that in the absence of disorder several of the optically dominant states of extended sheets still reflect the symmetries and phase relations of the cell eigenstates. In particular, the strongest state near 1645 cm^{-1} has a clear $|a-\rangle$ character, as recognized from its color map, which closely resembles an array of alternating red and blue columns. A second optically strong state near 1680 cm^{-1} is recognized as an $|a+\rangle$-type state through its representation as a stack of rows that alternate in color. Finally, a checkerboard color pattern is typical for the $|s-\rangle$-type state that occurs around $\sim$1705 cm^{-1}. A few other visible states are either recognized as higher wave vector states of the above ones or as mixtures of various unit cell states.

Energetic disorder has strong effects on the exciton states, as it destroys the translational symmetry (which is not perfect anyway, as a consequence of edge effects) and leads to localization of the exciton states. As we demonstrated, however, within their localization area, in particular, the states underlying the optically strongest peak in the linear spectrum clearly exhibit the $|a-\rangle$-type color map. In hindsight, this strongly suggests that the experimentally observed $\alpha-$ peak reported in ref 24 for poly-L-lysine and several β-sheet-containing proteins may be associated with the $|a-\rangle$ state. A more rigorous identification should involve an analysis of the color maps for these systems, using their known coordinates as input for constructing the exciton Hamiltonian.

The effects of energetic disorder on the linear spectrum of extended (two-dimensional) sheets reported here are quite generic: broadening and shifts of absorption lines follow power laws as long as the disorder strength is not too large. The powers found differ from those obtained for two-dimensional lattices, as a consequence of the strong anisotropic nature of the interactions in β-sheets. We have also found that disorder in the interactions, caused by random shifts of the oscillator positions, causes the dominant $|a-\rangle$ peak to shift to the blue, rather than the red. This marked difference with energetic disorder finds its origin in a decrease of the average TDC interactions in the presence of this type of disorder and is dominated by shifts in the direction of the peptide strands.

For the 2DIR spectrum, energetic disorder leads to stretching of the diagonal peaks in the diagonal direction, while the cross-peaks are stretched closer to the ω_1 direction. These two effects together lead to a Z-shape in the two-dimensional spectrum, which may be a useful signature of β-sheet content in experimentally observed spectra. Indeed, a Z-shape has been observed in the 2DIR spectra of various β-sheet-containing systems.[24] As opposed to our model results, the cross-peaks in the experimental spectra do not seem to exhibit any slanting relative to the ω_1 direction. As explained in section 4, this may result from a relatively large dynamic contribution in the broadening of the $|a+\rangle$ transitions in experiment. We also found that, for not-too-large disorder, the splitting between associated positive and negative features in the 2DIR spectrum scales inversely proportionally with the delocalization size of excitons in the β-sheet. Future studies should address the effects of dynamic disorder[49,50] and investigate whether in this case a similar scaling relation exists between the peak splitting and the exciton coherence size.

Acknowledgment. We would like to thank Prof. A. Tokmakoff for stimulating discussions and for sharing experimental results with us prior to publication.

References and Notes

(1) Drenth, J. *Principles of Protein X-ray Crystallography*; Springer-Verlag: Berlin, 1994.
(2) Wüthrich, K. *NMR of Proteins and Nucleic Acids*; Wiley: New York, 1986.
(3) Mukamel, S. *Acc. Chem. Res.* **1999**, *32*, 145.
(4) Mukamel, S. *Annu. Rev. Phys. Chem.* **2000**, *51*, 691.
(5) Khalil, M.; Demirdöven, N.; Tokmakoff, A. *J. Phys. Chem. A* **2003**, *107*, 5258.
(6) Krimm, S.; Bandekar, J. *Adv. Protein Chem.* **1986**, *38*, 181.
(7) Jackson, M.; Mantsch, H. *Crit. Rev. Biochem. Mol. Biol.* **1995**, *30*, 95.
(8) Loring, R. F.; Mukamel, S. *J. Chem. Phys.* **1985**, *83*, 2116.
(9) Tanimura, Y.; Mukamel, S. *J. Chem. Phys.* **1993**, *99*, 9496.
(10) Hamm, P.; Lim, M. H.; Hochstrasser, R. M. *J. Phys. Chem. B* **1998**, *102*, 6123.
(11) Woutersen, S.; Hamm, P. *J. Chem. Phys.* **2001**, *114*, 2727.
(12) Woutersen, S.; Mu, Y.; Stock, G.; Hamm, P. *Proc. Natl. Acad. Sci. U.S.A.* **2001**, *98*, 11254.
(13) Golonzka, O.; Khalil, M.; Demirdöven, N.; Tokmakoff, A. *J. Chem. Phys.* **2001**, *115*, 10814.
(14) Zanni, M. T.; Ge, N. H.; Kim, Y. S.; Decatur, S. M.; Hochstrasser, R. M. *Biophys. J.* **2002**, *82*, 66.
(15) Rubtsov, I. V.; Wang, J.; Hochstrasser, R. M. *J. Phys. Chem. A* **2003**, *107*, 3384.
(16) Asbury, J. B.; Steinel, T.; Stromberg, C.; Gaffney, K. J.; Piletic, I. R.; Goun, A.; Fayer, M. D. *Phys. Rev. Lett.* **2003**, *91*, 237402.
(17) Asbury, J. B.; Steinel, T.; Stromberg, C.; Gaffney, K. J.; Piletic, I. R.; Goun, A.; Fayer, M. D. *Chem. Phys. Lett.* **2003**, *374*, 362.
(18) Bredenbeck, J.; Helbing, J.; Behrendt, R.; Renner, C.; Moroder, L.; Wachtveitl, J.; Hamm, P. *J. Phys. Chem. B* **2003**, *107*, 8654.
(19) Moran, A. M.; Park, S. M.; Dreyer, J.; Mukamel, S. *J. Chem. Phys.* **2003**, *118*, 3651.
(20) Wang, J.; Hochstrasser, R. M. *Chem. Phys.* **2004**, *297*, 195.
(21) Abramavicius, D.; Zhuang, W.; Mukamel, S. *J. Phys. Chem. B* **2004**, *108*, 18034.
(22) Fang, C.; Wang, J.; Kim, Y. S.; Charnley, A. K.; Barber-Armstrong, W.; Smith, A. B., III; Decatur, S. M.; Hochstrasser, R. M. *J. Phys. Chem. B* **2004**, *108*, 10415.
(23) Cheatum, C. M.; Tokmakoff, A.; Knoester, J. *J. Chem. Phys.* **2004**, *120*, 8201.
(24) Demirdöven, N.; Cheatum, C. M.; Sung, H. S.; Khalil, M.; Knoester, J.; Tokmakoff, A. *J. Am. Chem. Soc.* **2004**, *126*, 7981.
(25) Chung, H. S.; Khalil, M.; Smith, A. W.; Ganim, Z.; Tokmakoff, A. *Proc. Natl. Acad. Sci. U.S.A.* **2005**, *102*, 612.
(26) Mirkin, N. G.; Krimm, S. *J. Am. Chem. Soc.* **1991**, *113*, 9742.
(27) Scheurer, C.; Piryatinski, A.; Mukamel, S. *J. Am. Chem. Soc.* **2001**, *123*, 3114.
(28) Ham, S.; Kim, J. H.; Lee, H.; Cho, M. *J. Chem. Phys.* **2003**, *118*, 3491.
(29) Choi, J. H.; Ham, S.; Cho, M. *J. Chem. Phys.* **2002**, *117*, 6821.
(30) Torii, H.; Tasumi, M. *J. Chem. Phys.* **1992**, *96*, 3379.
(31) Ham, S.; Cha, S.; Choi, J.; Cho, M. *J. Chem. Phys.* **2003**, *119*, 1451.
(32) Choi, J.; Ham, S.; Cho, M. *J. Phys. Chem. B* **2003**, *107*, 9132.
(33) Mukamel, S. *Principles of Nonlinear Optical Spectroscopy*; Oxford University Press: Oxford, 1995.
(34) In ref 23, this state appears at 1641 cm^{-1}. The discrepancy is because, in the current calculations, we only account for the eight strongest interactions J_{nm} (see Figure 2).
(35) Miyazawa, T. *J. Chem. Phys.* **1960**, *32*, 1647.
(36) Miyazawa, T.; Blout, E. R. *J. Am. Chem. Soc.* **1961**, *83*, 712.
(37) Chirgadze, Y. N.; Nevskaya, N. A. *Biopolymers* **1976**, *15*, 607.
(38) Schreiber, M.; Toyozawa, Y. *J. Phys. Soc. Jpn.* **1982**, *51*, 1528.
(39) Fidder, H.; Knoester, J.; Wiersma, D. A. *J. Chem. Phys.* **1991**, *95*, 7880.
(40) Bakalis, L. D.; Knoester, J. *J. Phys. Chem. B* **1999**, *103*, 6620.
(41) Bakalis, L. D.; Knoester, J. *J. Lumin.* **1999**, *83/84*, 115.

(42) Dahlbom, M.; Pullerits, T.; Mukamel, S.; Sundström, V. *J. Phys. Chem. B* **2001**, *105*, 5515.
(43) Chachisvilis, M.; Kühn, O.; Pullerits, T.; Sundström, V. *J. Phys. Chem. B* **1997**, *101*, 7275.
(44) Didraga, C.; Knoester, J. *J. Chem. Phys.* **2004**, *121*, 10687.
(45) Knoester, J. *J. Chem. Phys.* **1993**, *99*, 8466.
(46) Rubtsov, I. V.; Wang, J.; Hochstrasser, R. M. *J. Chem. Phys.* **2003**, *118*, 7733.
(47) Thouless, D. J. *Phys. Rep.* **1974**, *13*, 93.
(48) Juzeliūnas, G. *Z. Phys. D* **1988**, *8*, 379.
(49) Kwac, K.; Cho, M. *J. Chem. Phys.* **2003**, *119*, 2247.
(50) Kwac, K.; Cho, M. *J. Chem. Phys.* **2003**, *119*, 2256.